# Classification of Relative Object Size from Parieto-occipital Hemodynamics Using Type-2 Fuzzy Sets

Amiyangshu De
Department of Bioscience and Bioengineering
Indian Institute of Technology
Jodhpur, India
de.1@iitj.ac.in

Mousumi Laha
Department of Electronics and Telecom. Engineeringline
*Jadavpur University*
Kolkata, India
lahamou@gmail.com

Amit Konar
Department of Electronics and Telecom. Engineeringline
*Jadavpur University*
Kolkata, India
konaramit@yahoo.co.in

Atulya K. Nagar
Mathematics and Computer Science Department
Liverpool Hope University
United Kingdom
nagara@hope.ac.uk

***Abstract*— During the past two decade researchers have been exploring the mechanism of object shape and depth perception using EEG and fMRI. However, the underlying cortical process of perceiving different object sizes from a constant visual distance has never been explored. This paper provides a novel understanding of relative object size classification based on direct measure of parieto-occipital hemodynamics using functional near infrared spectroscopy (fNIRS). The cortical response is recorded from subjects engaged in visual perception task of relative object size. The signal is preprocessed (artifact removal) for construction of 176 features, which are thus reduced to 22 features using particle swarm optimization (PSO) technique. The reduced features are subsequently fed into an interval type -2 fuzzy set to classify the perceived objects (based on the underlying hemodynamic data) into three different classes: LARGE, MEDIUM and SMALL. Experimental analysis shows that the proposed feature-selection and classification framework attain higher classification accuracy which reaches over 87% in the classification of large objects. Analysis, further undertaken to know the underlying neurovascular mechanisms, reveals a distinct dorso-ventral shift (shall-medium-to-large) in parieto-occipital hemodynamic load which can be observed from the topographic brain activation. The average activation shifts are measured as 73.35 degrees in the right hemisphere compared to 93.71 degrees in the left hemisphere. The experimental outcomes could provide a novel measure in cortical hemodynamic features based perception of object size. In future, it could provide justification towards the visually challenged persons with perceptual difficulties.**

***Keywords—fNIRS, Meta-heuristic feature selection, Relative object size, Type-2 fuzzy classifier.***

## I. Introduction

In the past 2 decades, functional neuro-imaging based brain computer interface (BCI) research has gained high momentum as an important tool to decode the mystery of human perception. Visual perception in modern hominids is considered to be the most significant bio-mechanism to acquire information from the external world to understand meaning of the perceived information in the neural circuits of the brain. The engagement of neural population representing the task of perception is dependent on the speed of metabolism – the process which requires oxygen to produce energy from blood glucose [1], [2]. The blood oxygen level dependent (BOLD) activity is also a measure of the spatio-temporal distribution of energy supply in the engaged brain regions [3]. A functional near-infrared spectroscopy (fNIRS) measures blood oxy-hemoglobin and de-oxy-hemoglobin levels over the brain regions related to the optodes positioning. This study attempts to predict the change in spatio-temporal hemodynamic of subjects engaged in visual stimulus based relative object size perception (large, intermediate and small) of geometric objects. The background studies on visual perception prior to the experiments provide us traces of literates on fNIRS based analysis of depth perception and object recognition – for example, the stereoscopic dynamic depth perception by Ward and associates [4], understanding the visual fatigue in binocular depth perception by Cai et al. [5], role of lateral occipital cortex in determining object shape [6]. Additionally, we can report few functional neuroimaging based research in the similar direction – understanding the 3D shape in the human visual cortex from motion [7], representation of object distance of 2D objects based on monocular cues [8], correlation between monocular and binocular depth cues from natural stereoscopic images [9]. One closely related research to the objective of this paper is reported by Tanaka and Fujita [10] from a cellular neuroscience viewpoint using electrophysiology. Additionally, we can report effective application of type-2 fuzzy sets in brain machine interface (BMI) for humanoid robot [11] and classification of cognitive engagement in different perceptual tasks with better performance from conventional approaches [12].

However, recent studies have not pointed their focus towards understanding the cortical mechanism of perceiving relative object size. In short, how object size is perceived – small, medium and large from a fixed visual distance in the cortical areas is still an open area of research. In this aspect, functional near infrared spectroscopy could reveal the cortical mechanism of the perception of object size based on the acquired hemodynamic response of the brain. The principle of understanding the hemodynamic pattern of visually perceiving object shapes is crucial as it can provide important direction to the treatment with perceptual disabilities and improper vision. The research ambition of this paper to classify parieto-occipital hemodynamic features, recorded by fNIRS, related to visually perceived object sizes: large, medium and small. The recorded signals are preprocessed, filtered to remove physiological and environmental artifacts. We use particle swarm optimization (PSO) to reduce the high dimensional feature sets into reduced dimensions which is fed into an interval type-2 fuzzy classifier object sizes. The recorded fNIRS signals may undergo wide range of intra as well as inter session unpredictability which causes uncertainty among the feature sets. As, type-2 fuzzy classifier showed encouraging results dealing with the

978-1-7281-6932-3/20/$31.00 ©2020 IEEE

uncertainty within and across the sessions, we adopt it for this current research. Additionally, fuzziness becomes visible in the present circumstances, due to interpersonal perceptual variability in conceptualize visual objects, which could be well classified by using type-2 fuzzy sets. So, in brief, though persons have individual measure of perceiving objects, the generalized pattern of size perception can be revealed. Here, lies the definite gain from type-2 fuzzy classifier in determining pattern from hemodynamic response. The novelty of this paper lies in the design of type-2 fuzzy classifier in this particular context. Additional merit of the paper lies in the meta-heuristic feature selection.

Experiments undertaken confirm that the proposed Interval Type-2 fuzzy (IT2Fs) classification technique outperform to its competitors by a large margin. Statistical test also confirms the superiority of the proposed technique with its competitors

The paper is organized in the following ways: section II contains the theoretical aspect of the research objective, interval type-2 fuzzy classifier and PSO based meta-heuristic feature selection. Section III reports the experimental outcomes and results. Section IV concludes this research.

## II. PRINCIPLES AND METHODS

This section provides the underlying theoretical basis of this research problem, tools and techniques developed to answer the given problem. The following measures are taken in this section: (a) theoretical basis of relative size perception and role of parieto-occipital cortex, (b) preprocessing and artifact removal, (c) PSO based meta-heuristic feature selection, (d) classification of the hemodynamic features into perceived object sizes. The stated approaches are reported below:

### *A. Theoritical Basis: Relative Object Size and Parieto-occipital Cortex*

Size can be considered as a salient feature of real-world objects, for instance, large objects are considered as landmarks and relatively stagnant in their position, whereas smaller objects are considered rather movable. As mentioned by previous researchers that visual cortex respond differently to large versus small objects, the fMRI based findings by Julian *et al.* about differential spatial selectivity to large versus small objects and the varied strength of regional activation in this process provides the underlying basis of size perception [13]. Among the considered factors of size perception, the most important is the visual angle formed by the object in the retina. Considering all other parameters as similar, the object that form larger angle on the retina appears as large. The visual angle is largely dependent on two factors: (a) the real object size, (b) the distance of the object from the eye [14]. In visual perception, the transformation of neural signals occur in the retina, occipital area V1 and extra-striate cortex to create pattern of the represented information [15]. The visual pathway for object recognition is reported to be from the projection to temporal cortex [16]. However, beyond the association of occipital and temporal cortex, parietal cortex plays significant role in visual grouping [17] and object based attention [18]. Vaziri-Pashkam and Xu revealed that the object category representation based on both occipito-temporal and posterior parietal cortex [19].

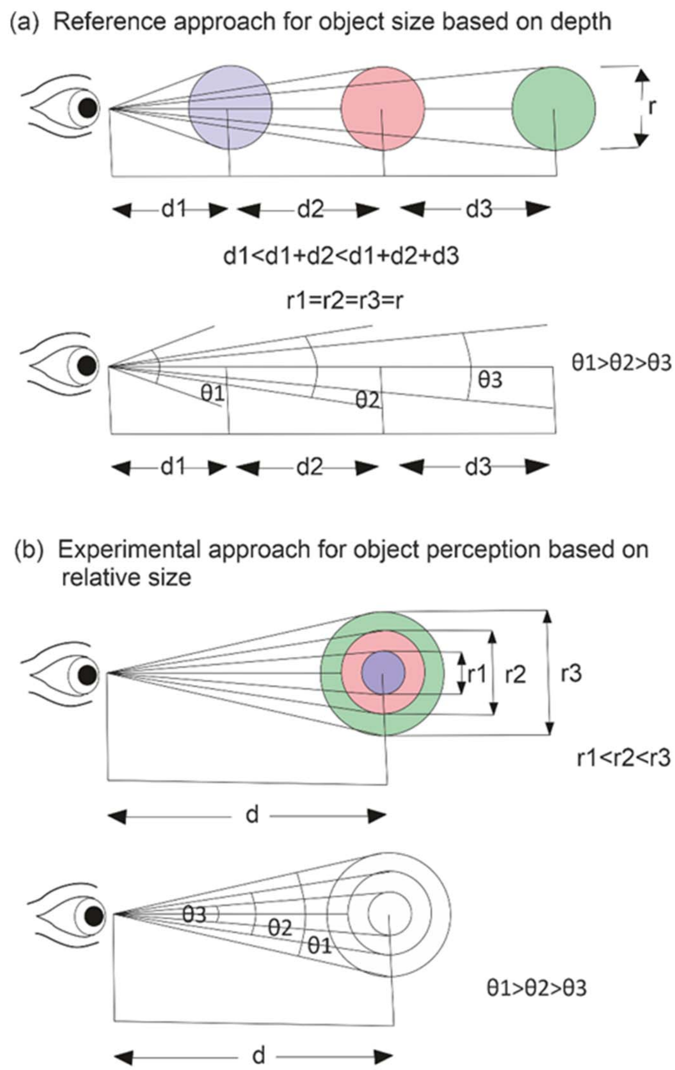


Fig.1 Theoretical framework for relative object size perception

The hypothesized objective in this paper is to understand the cortical mechanism of perceiving object size keeping the visual distance as constant. Conventional framework demonstrates the visual distance ($d$) and the visual angle ($\theta$), both changes for measuring object size. Here, if

$$d_1 < (d_1 + d_2) < (d_1 + d_2 + d_3)$$

and

$$\theta_1 > \theta_2 > \theta_3$$

then,

$$object_1 > object_2 > object_3$$

In the proposed objective (Fig.1), we keep object distance as constant ($d$) as:

$$d_1 = d_2 = d_3$$

However, in the diameter of the objects play a crucial role, where,

$$r_1 < r_2 < r_3$$

and the visual angle formed in the retina as:

$$\theta_1 > \theta_2 > \theta_3$$

In this aspect, the perceived objects size is to be:

$$object_1 > object_2 > object_3$$

*B. Pre-processing*

The fNIRS signals obtained from all the channels are processed using elliptical band pass filter of order 10, where the cut off frequency is kept between 0.01-0.2 Hz [20] to get rid of major physiological artifacts like Mayer's effect due to vascular blood flow (~0.1 Hz), heart beats (1-1.5 Hz), respiration (0.2-0.5 Hz) [21]. Eye-blinking (0.5-3 Hz) and muscle movements [22]. Additionally, an independent component analysis (ICA) is performed to restore independent components of hemodynamic responses for the 22 fNIRS channels from the mixed cortical signals [23].

*C. Data Normalization*

Due to inter and intra session variability of fNIRS signals, the recorded data is needed to be scaled. Consider, $M_{i,HbO}$ is the concentration of oxy-hemoglobin (HbO) and $M_{i,HbR}$ is the concentration of de-oxy-hemoglobin (HbR). The maximum and minimum concentrations of HbO are considered as $M_{HbO}^{max}$ and $M_{HbO}^{min}$ respectively. The similar notation follows for the maximum and minimum concentrations of HbR also. The HbO data is normalized using the following measure:

$$M_{i,HbO}^{*} = \left(M_{i,HbO} - M_{HbO}^{min}\right) / \left(M_{HbO}^{max} - M_{HbO}^{min}\right) \qquad (1)$$

Similarly, we normalize the HbR data as the following. The criterion used for HbR is similar to that used in HbO.

$$M_{i,HbR}^{*} = \left(M_{i,HbR} - M_{HbR}^{min}\right) / \left(M_{HbR}^{max} - M_{HbR}^{min}\right) \qquad (2)$$

Due to the normalization, we found all the data sets are normally distributed - all the data points lie within three standard deviations range values from the mean $(\mu \pm 3\sigma)$ [24].

*D. Feature Extraction*

The below mentioned 8 features are extracted from the 22 fNIRS channels that produce a set of 22×8 =176 features for each participant. So, for 18 participants, we have a feature dimension of 18×176 (for single object class), where 18 is the number of participants and 176 is features for each participant.

- $f_1$ Mean HbO concentration
- $f_2$ Mean HbR concentration
- $f_3$ Total Hemoglobin (HbO+HbR) conc.
- $f_4$ Latency of HbO response initiation
- $f_5$ Rise time of HbO response
- $f_6$ Peak amplitude of HbO response
- $f_7$ Recovery time of HbO response
- $f_8$ Width at half maximum peak of HbO response

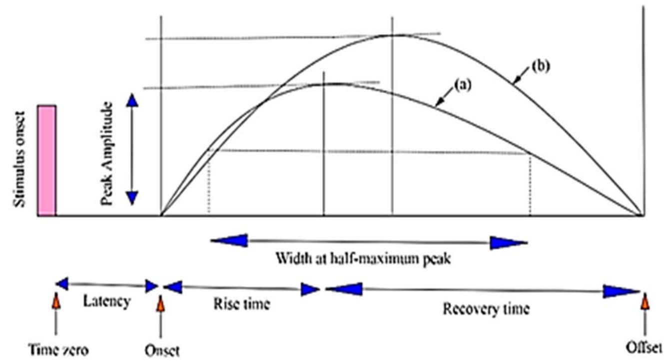


Fig.2 Representative Scheme of feature construction (shown for signal 1 (a) Distribution pattern of signal 1, (b) Distribution pattern of signal 2

The representative image of feature construction is shown in Fig.2.

*E. Training Instances for the Object Classes*

This experiment is basedon3 different object classes: LARGE, MEDIUM and SMALL. Each participant undergoes 3 trials/object stimuli of 3 different sized objects (same shape) and for a set of 4 different geometric shaped objects. So, all the 18 subjects generate 18 × 3 (trials/object) 3 (3 different object classes) × 4 (4 set of different geometric object shapes) = 648 total training instances (216 trials for one object class).

*F. Meta-heuristic Feature Selection*

The 176 dimensional features are reduced to 22 vector dimensions using meta-heuristic feature selection. In this concern, the feature selection is performed as an optimization problem after satisfying the following two criteria: (a) the city block distance between the $m^{th}$ vector and $n^{th}$ centroid to be minimized whereas (b) the distance between centroids to be maximized.

More specifically, consider $\vec{a}_m^{\,x} = \left\{\vec{a}_{m,1}^{\,x}, \ldots\ldots\ldots \vec{a}_{m,R}^{\,x}\right\}$ is the $m^{th}$ feature vectors which has $R$ components and belongs to class $x$, $b_n^x$ and $b_n^y$ are the $n^{th}$ elements class centroids of the respective classes $x$ and $y$. The objective functions are defined below in equation 3 and 4.

$$G1 = \sum_{c=1}^{P} \sum_{m=1}^{Q} \sum_{n=1}^{R} \left|a_{m,n}^{x} - b_n^x\right| \qquad (3)$$

$$G2 = \sum_{k=1,k\neq c}^{P} \sum_{c=1}^{P} \sum_{n=1}^{R} \left|b_n^x - b_n^y\right| \qquad (4)$$

Here, $P$ indicates total number of classes, $Q$ for number of data points and $R$ refers to the number of features. The objective function $G3$ (equation 5) is developed to jointly optimize objective functions $G1$ and $G2$.

$$G3 = G1 - \beta \times G2 \qquad (5)$$

Or,

$$G3 = \sum_{c=1}^{P} \sum_{m=1}^{Q} \sum_{n=1}^{R} \left|a_{m,n}^{x} - b_n^x\right| - \beta \times \sum_{k=1,k\neq c}^{P} \sum_{c=1}^{P} \sum_{n=1}^{R} \left|b_n^x - b_n^y\right| \qquad (6)$$

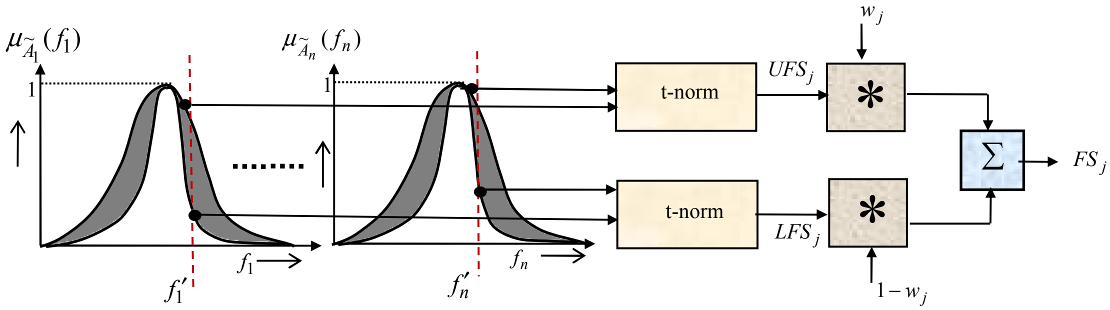


Fig.3. Architecture of Proposed Classifier

Here, $\beta$ is the Lagrange's multiplier which scales $G1$ and $G2$ into the same order of magnitude. The best $r$ features are selected among the $R$ features after optimizing equation (5) using particle swarm optimization (PSO) [25].

### G. *Interval Type-2 Fuzzy set induced Classification of Object Size.*

The hemodynamic data produced has diverse ranges due to inter and intra session variability. Additionally, the interpersonal variability of brain signals come into account. In this regard, interval type-2 fuzzy classifier (IT2FC) has shown promising results in handling the uncertainty emerged within and during sessions.

We develop IT2FC to classify the 22 dimensional data points into three relative object size classes: LARGE, MEDIUM and SMALL. The example classifier rule is mentioned in Table 1.

TABLE-I
REPRESENTATIVE IT2FS INDUCED CLASSIFICATION RULES FOR MEASURING RELATIVE OBJECT SIZE.

| | |
|---|---|
| Rule I | IF for all the selected features $f_1, f_3, f_3, f_7, f_8$ are HIGH and $f_5$ is INTERMEDIATE and $f_2$, $f_4$ are LOW, THEN object size is LARGE. |
| Rule II | IF for all the selected features $f_3, f_5, f_8$ are HIGH and $f_1$, $f_2$, $f_4$, $f_6$ are INTERMEDIATE and $f_7$ is LOW, THEN object size is MEDIUM. |
| Rule III | IF for all the selected features $f_4, f_5$ are HIGH and $f_8$ is INTERMEDIATE and $f_1$, $f_2$, $f_3$, $f_3$, $f_7$ are LOW, THEN object size is SMALL. |

Let, $f_1, f_2, ...., f_n$ be the $n$ number of selected features acquired from the specific brain lobes involved in the present cognitive task. Let $\widetilde{A}_i$ for $i$=1 to $n$ be an interval type-2 fuzzy sets (IT2FS) defined as $[\overline{\mu}_{\widetilde{A}_i}, \underline{\mu}_{\widetilde{A}_i}]$ for a given linguistic variable $f_i$ . Here, both intra-session and inter-session variations have been considered in $f_i$ after stimulating a subject with a specific visual stimulus. To construct a type-1 Gaussian Membership Function (MF), the mean ($M$) and Variance $(Var_i^2)$ of the intra-session variations has been considered, where the center of the base is located at $M$ and two extremities are located at $M \pm 3 \times \sigma$.

Now to accommodate, the daily variations in result, the maximum of $d$ such Type-1 MF have been taken to construct the Upper Membership Function (UMF) of the type-1 fuzzy set.

$$UMF_j = \max(\overline{\mu}_{\widetilde{A}_1}(f_1), \overline{\mu}_{\widetilde{A}_2}(f_2), ..., \overline{\mu}_{\widetilde{A}_n}(f_n)) = \overline{\mu}_{\widetilde{A}_i}(f_i) \quad (7)$$

Then, the Lower Membership Function (LMF) is constructed by taking the concentration of UMF, represented as

$$LMF_j = con(\widetilde{A}_i) = (\overline{\mu}_{\widetilde{A}_i}(f_i))^2 \quad . \quad (8)$$

Although there exists several alternatives to construct the IT2FS, the above methodology has been adopted for its simplicity and less intra-session variability.

Next, we consider a classifier rule $j$ for class $j$, which is defined as follows.

*If* $f_{1,j}$ *is* $\widetilde{A}_{1,j}$ *and* $f_{2,j}$ *is* $\widetilde{A}_{2,j}$ *and ... and* $f_{n,j}$ *is* $\widetilde{A}_{n,j}$, *then class* = $j$.

Let the measurements points be $f_1 = f_1', f_2 = f_2', ..., f_n = f_n'$.

The following steps are undertaken to compute the firing strength of class $j$.

1) Computation of Upper Firing Strength (UFS) of rule $j$ depicted by

$$UFS_j = \min[\overline{\mu}_{\widetilde{A}_1}(f_1), \overline{\mu}_{\widetilde{A}_2}(f_2), ..., \overline{\mu}_{\widetilde{A}_n}(f_n)] \quad (9)$$

2) Computation of Lower Firing Strength (LFS) of rule $j$ illustrated by

$$LFS_j = \min[\underline{\mu}_{\widetilde{A}_1}(f_1), \underline{\mu}_{\widetilde{A}_2}(f_2), ..., \underline{\mu}_{\widetilde{A}_n}(f_n)] \quad (10)$$

3) The product of the weighted sum of $UFS_j$ and $LFS_j$ is taken to compute the firing strength of rule $j$. The weights lie between [0, 1] hence, one weight is $w_j$ and the other weight is $1 - w_j$ . Thus, the firiging Strength ($FS$) for class $j$ will be,

$$FS_j = w_j . UFS_j + (1 - w_j) . LFS_j . \quad (11)$$

Finally, Evolutionary algorithm has been utilized for optimal selection of the weights. The weights of all rules together form a vector. This vector is adopted to optimize the fitness function $J = \underset{j}{\forall} CA_j$, where $CA_j$ is the classification accuracy of rule $j$ with an aim to maximize the classification accuracy for all classes. The architechture of the proposed classifier has been depicted in Fig. 1.

## III. EXPERIMENTS AND RESULTS

This section summarizes the experimental set-up, analytical results, interpretation and discussion.

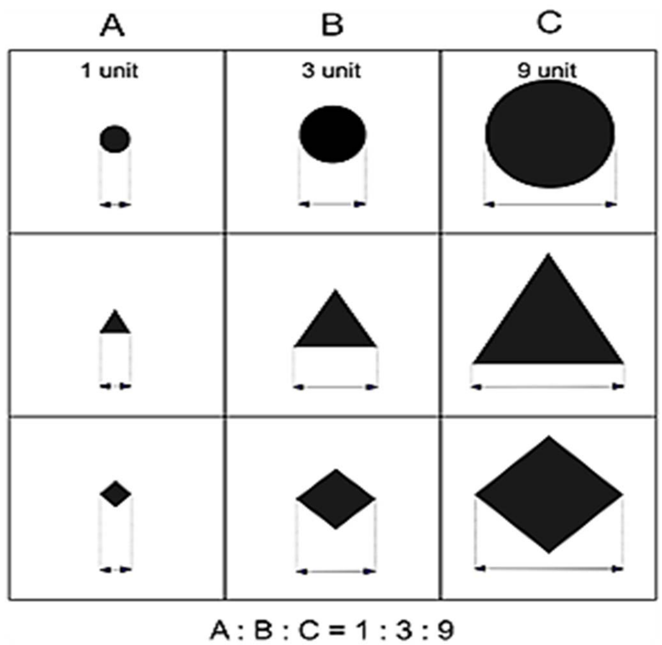


Fig.4. A representative framework of stimulus presentation for relative size perception. The object size is maintained as small: medium: large = 1:3:9.

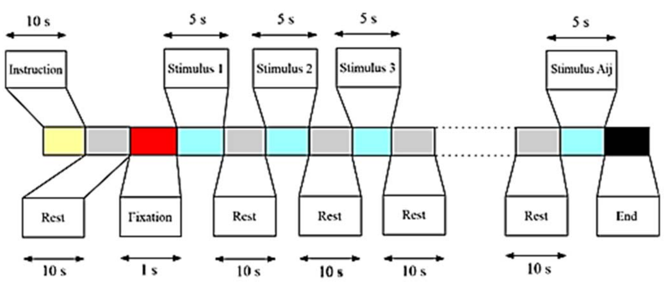


Fig.5. Scheme of stimulus presentation for relative object size perception.

### A. Experimental Set-up

Eighteen volunteers of mean age 23.6 (SD ±1.99) and with normal or corrected vision participated in this experiment. None of the participants had present or past history of neurological or vascular diseases. A visual stimulus of geometric objects of sizes SMALL (1): MEDIUM (3): LARGE (9) is presented over the computer screen at a visual distance of 60 cm. Four different geometric object shapes are selected to be presented as visual stimulus with varied size. The visual stimulus for perceiving the relative size is presented in a window of 5 seconds, followed by a 10 seconds gap. The relative size perception task is repeated thrice for each subjects. The representative stimulus for this relative size perception task is presented in Fig.4 and the scheme of stimulus presentation is shown in Fig.5.

A continuous wave fNIRS (NIRScout) with sampling frequency ~8 Hz is used to capture the parieto-occipital hemodynamic response of the subjects engaged in the relative object size perception task. 8 IR light emitters and 7 detectors

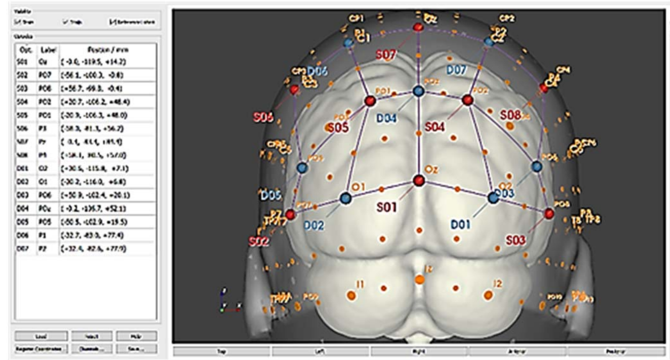

Fig.6. Optodes positioning in the fNIRS cap consisting of 8 emitters and 7 recorders, forming total 22 channels.

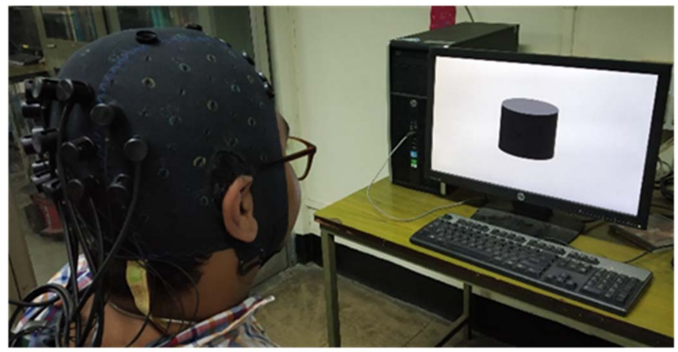

Fig.7. Capturing of parieto-occipital hemodynamic response during relative object size perception task performance.

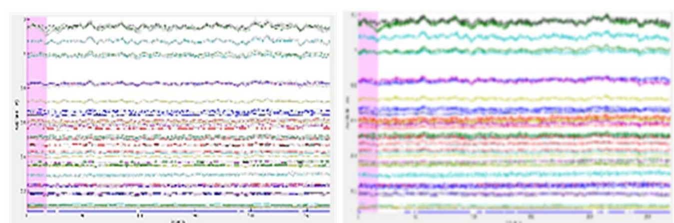

(a) (b)

Fig.8. Acquired HbO signals during the task performance (a) before and (b) after filtering using elliptical filter.

formed 22 channels in the parieto-occipital brain regions. The position of the optodes over the head cap is shown in Fig.6. Data acquisition, analysis and visualization is done using nirsLAB software. For each instances, base line response is removed prior to data acquisition. Fig.7 shows capturing parieto-occipital hemodynamic from a subject engaged in visual stimulus based relative size perception task. The raw hemodynamic response from the 22 channels and the signal property after using elliptical band pass filter is shown in Fig.8 represents the HbO signals during the time span of task performance (a) before and (b) after using elliptical band pass filter. Data analysis and classification is performed using MATLAB 2015b software.

### B. Biological Implication: Distribution of HbO Load

Diverse hemodynamic response is observed in perceiving different object sizes of provided geometric shapes. In order to understand the hemodynamic load distribution in the parieto-

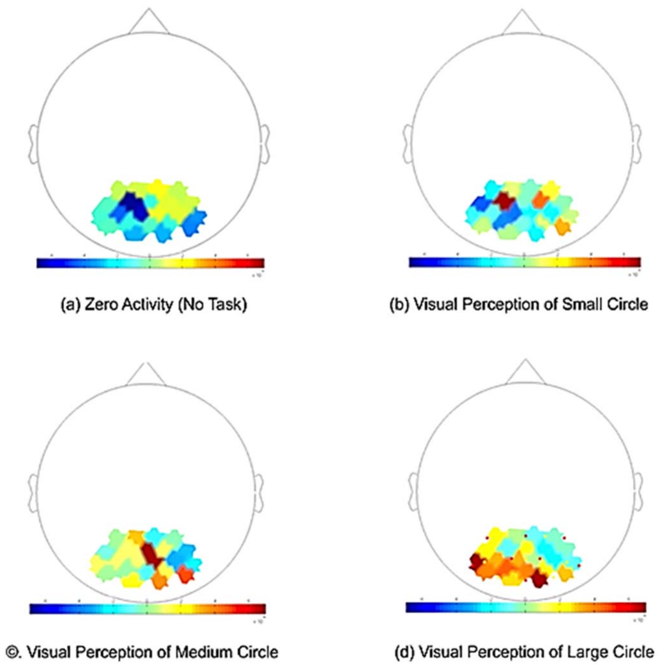


Fig. 9. Voxel representation of mean HbO concentration during the performance of visual perception of relative object size (representative for relative size perception of circles). The figure scale measured as $6 \times 10^{-8}$. (a) Hemodynamic load distribution during performing no task, (b) perceiving small circle, (c) perceiving medium circle and (d) perceiving large circle.

occipital cortex. We use nirsLAB to get the mean HbO concentration over the 22 voxels during perception of NO object, SMALL, MEDIUM and LARGE objectsrespectively. Figure 9 represents the mean HbO distribution pattern among the voxels during the perception of relative size of circles, where, dark red and deep blue colors represent highest level of cortical activation and deactivation respectively. From Fig.9, it is evident that visual perception of larger objects produce broader activation of the parieto-occipital regions compared to medium and smaller objects. Considering the dorsal versus ventral stream dichotomy of visual perception [26], [27], [28], we observe small objects are projected in the dorsal visual path (dealing with object location and maintaining movements through visual control [27]) near the inferior parietal lobule, the objects in the class of medium size majorly activates superior parietal lobule along with distributed lateral occipital activation. However, objects with large size caused major activation in the ventral occipital cortex and spread activation in the lateral occipital cortex (visual association area). This indicates large objects perception could be related to the ventral

TABLE II. MEAN CLASSIFICATION ACCURACIES

| Relative Object Size Class | PCA L-SVM | PCA RBF-SVM | PCA-kNN | PCA-LDA | PCA-IT2FS | PSO-IT2FS |
|---|---|---|---|---|---|---|
| Small | 73.97 | 76.11 | 70.23 | 66.17 | 79.38 | 84.76 |
| Medium | 72.06 | 73.29 | 69.79 | 63.29 | 80.41 | 81.03 |
| Large | 74.09 | 78.60 | 68.04 | 68.46 | 83.93 | 87.52 |

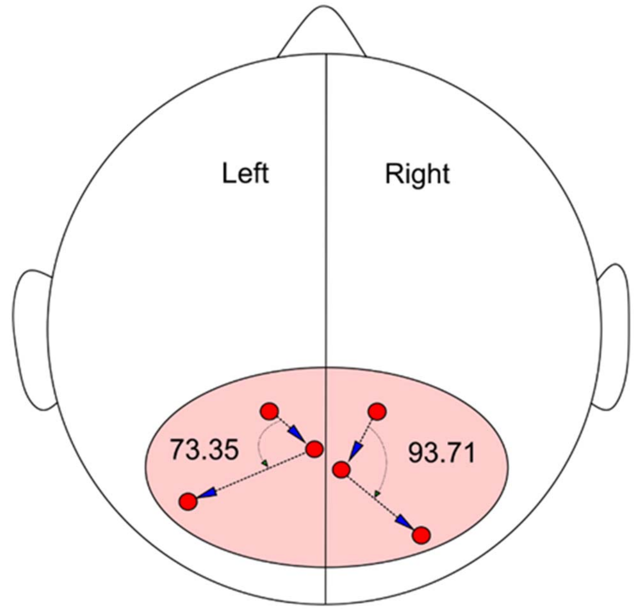


Fig. 10. Average Angular shift of central hemodynamic load (HbO concentration) in the parieto-occipital brain areas in perceiving relative object sizes (from small – medium – large). The blue arrows indicate the dynamic shift in central cognitive load during visual perception task from small objects to large objects.

TABLE-III
CONFUSION MATRIX OF
PSO BASED FEATURE SELECTION INDUCED IT2FS

| Predicted Class / Actual Class | Small | Medium | Large |
|---|---|---|---|
| Small | 84.76 | 7.87 | 7.40 |
| Medium | 6.94 | 81.03 | 12.03 |
| Large | 7.40 | 5.09 | 87.52 |

route of visual system which is mostly related to object identity [27]. Additionally, small objects initiates activation in Broadmann area 7 (A) and 39 which have functions in spatial location of objects and language processing (also reasoning) respectively [29]. The intermediate sized objects activates visual association areas (Broadmann area 17, 18 and 19), which is a role in object pattern detection [30]. Further, Broadmann's area 19 and 37 get major activation in perceiving larger objects. The area 37 has specific role in object identification (naming) [31]. However, we observe higher cortical activation in the left hemisphere compared to the right during object size perception.

### *C. Angular Measure of Shift in parieto-occipital Activation.*

The hemodynamic load distribution in the parieto-occipital region has shown angular pattern in perceiving objects from smaller to larger in size. Fourteen subjects among the participants shows distinct pattern of cortical distribution of hemodynamic load in perceiving small, medium and large objects. Considering the voxels of highest activation in small, medium and large objects, we construct an angular projection of this activation pattern: in the left hemisphere, the observed mean angular shift is 93.71 (SD±8.15) degree whereas, it is found to be 73.35 (SD±5.61) degree in the right hemisphere.

TABLE-VI: CLASSIFIERS' RANKING

| Class Dataset | PCA L-SVM | PCA RBF-SVM | PCA-kNN | PCA-LDA | PCA-IT2FS | PSO-IT2FS |
|---|---|---|---|---|---|---|
| Small | 4 | 3 | 5 | 6 | 2 | 1 |
| Medium | 4 | 3 | 5 | 6 | 2 | 1 |
| Large | 4 | 3 | 6 | 5 | 2 | 1 |
| $\sum T_i^2$ | 48 | 27 | 86 | 97 | 12 | 1 |

Fig. 10 shows a representative diagram of the angular shift in perception of relative object size.

### *D. Classification of Perceived Object Size*

The classification accuracy of the proposed feature selection (PSO) based IT2FS and comparison with the existing feature selector-classifier techniques are summarized in Table II. We select best 22 features using PSO from the 176 dimensional feature matrix and apportion the data in a ratio of 60:20:20 as training set, validation set and test set. The validation set is used to evaluate results from the training set. As the model passed the validation set, we use the test set for classifiers' performance.

The existing feature selector-classifiers considered in this table are –Principal Component Analysis (PCA) based Linear Support Vector Machine (L-SVM), Support Vector Machine with Radial Basis Function (RBF-SVM), k-Nearest Neighbor (kNN), and Linear Discriminant Analysis (LDA), IT2FS. It is obvious from Table.2 that our proposed PSO based feature selector induced IT2FS classifier performs better with respect to classification accuracy.

Table III. enlists individual class performance of the proposed meta-heuristic feature selection induced IT2FS classifier from confusion matrix to distinguish three different perceived object size classes: LARGE, MEDIUM and SMALL. Our proposed feature selector – classifier delivers classification accuracy 81% as the least value, whereas, it tends to reach more than 87% in classifying LARGE objects class.

### *E. Statistical Validity of Classifiers' Ranking*

Friedman's non-parametric test is a two-way analysis of variance by rank. Friedman's test ranks the classification algorithms on each data sets considering their classification accuracies. The Friedman statistics score $F_R$ is computed using the following formula –

$$F_R = \frac{12}{m \times n(n+1)}[(T_1^2 + T_2^2 + \cdots + T_i^2) - 3m(\text{n}+1)] \quad (12)$$

Where, m is the number of data sets (number of object size classes) and $n$ indicates the number of classification algorithms, $T_n$ is the rank of the classifier in the $i^{th}$ class of the data set [32]. Table-IV reports classifiers' ranking. In this concern, we hypothesize as the following:

$H_0$: There is no significant different in classification accuracy between the classification algorithms.

$H_1$: Significant difference in classification accuracy exists between the classification algorithms.

From equation 10, we obtain $F_R$=19.81, which is $>\chi^2_{5,0.05}$ =11.07 at 5 $df$ and 95% confidence level. So, $H_0$ is rejected and the classifiers can be ranked according to classification accuracies.

## IV. CONCLUSION

This paper offers a new conceptual framework to classify relative object size from different geometric object shapes using fNIRS based parieto-occipital hemodynamic features. The uniqueness of this paper lies in the design of intelligent meta-heuristic feature selection algorithm and IT2FS induced classification of visually perceived object sizes into three output classes: SMALL, MEDIUM and LARGE. Experimental analysis indicates the proposed feature selector- classifier performs superior than conventional techniques. Biological underpinning of the cortical mechanism in perceiving object size is also a significant inclusion in this paper. From voxel plots obtained from fnirsLAB it is evident that cortical activation shifts from dorsal to ventral visual path when the visual perception of object size changes from small – medium – large. The engagement of interior parietal lobule, association visual cortex and ventral occipito-temporal path could play crucial role in inking between object size perception, language and memory. For instance, inferior parietal cortex essentially activates in perceiving smaller objects, whereas, the activation moves towards ventral path (Broadmann's area 37) during perception of larger objects. However, we could not catch the temporal pattern of hemodynamic response during the task of relative object size perception, which, possibly, could be better understood with the help of EEG-fNIRS based hybrid system.

## ACKNOWLEDGMENT

The authors acknowledge the financial support provided by MHRD, Indian Institute of Technology, Jodhpur and JU-RUSA 2.0 project (MHRD) awarded to Jadavpur University, Kolkata, India.

## REFERENCES

[1] A. B. Scholey, S. Harper and D. O. Kennedy, "Cognitive Demand and Blood GLucose," *Physiology and Behaviour,* vol. 73, no. 4, pp. 585-592, 2001.

[2] M. A. Mintun, B. N. Lundstorm, A. Z. Snyder, A. G. Vlassenko, G. L. Shulman and M. E. Raichle, "Blood flow and oxygen delivery to human brain during functional activity: Theoretical modeling and experimental data," *PNAS,* vol. 98, no. 12, pp. 6859-6864, 2001.

[3] V. Scarapicchia, C. Brown, C. Mayo and J. R. Gawryluk, "Functional Magnetic Resonance Imaging and Functional Near-Infrared Spectroscopy: Insights from Combined Recording Studies," *Frontiers in HUman Neuroscience,* vol. 11, p. 419, 2017.

[4] L. M. Ward, G. Morison, W. A. Simpsom, A. J. Simmers and U. Sahani, "Using Functional Near Infrared Spectroscopy (fNIRS) to Study Dynamic Stereoscopic Depth Perception," *Brain Topography,* vol. 29, pp. 515-523, 2016.

[5] T. Cai, H. Zhu, J. Xu, S. Wu, X. Li and S. He, "Human cortical neural correlates of visual fatigue during binocular depth perception: An fNIRS study," *PLoS One,* vol. 12, no. 2, p. e0172426, 2017.

[6] L. L. Emberson, S. L. Crosswhite, J. E. Richards and R. L. Aslin, "The Lateral Occipital Cortex Is Selective for Object Shape, Not

Texture/Color, at Six Months," *J. Neurosci,* vol. 37, no. 13, pp. 3698-3703, 2017.

[7] S. O. Murray, B. A. Olshausen and D. L. Woods, "Processing Shape, Motion and Three-dimensional Shape-from-motion in the Human Cortex," *Cerebral Cortex,* vol. 13, no. 5, pp. 508-516, 2003.

[8] M. E. Berryhill and I. R. Olson, "The representation of object distance: evidence from neuroimaging and neuropsychology," *Frontiers in Human Neuroscience,* p. doi.org/10.3389/neuro.09.043.2009, 2009.

[9] F. P. Fischmeister and H. Bause, "Neural correlates of monocular and binocular depth cues based on natural images: A LORETA analysis," *Vision Research,* vol. 46, no. 20, pp. 3373-3380, 2006.

[10] S. Tanaka and I. Fujita, "Computation of Object Size in Visual Cortical Area V4 as a Neural Basis for Size Constancy," *J Neurosci,* vol. 35, no. 34, pp. 12033-12046, 2015.

[11] J. Andreu-Perez, F. Cao, H. Hagras and . G.-Z. Yang, "A Self-Adaptive Online Brain-Machine Interface of a Humanoid Robot Through a General Type-2 Fuzzy Inference System," *IEEE Transactions on Fuzzy Systems,* vol. 99, p. 1, 2016.

[12] S. Datta, A. Khasnobish, A. Konar and D. N. Tibarewala, "Cognitive Activity Classification from EEG Signals with an Interval Type-2 Fuzzy System," in *Advancements of Medical Electronics*, New Delhi, Springer, 2015, pp. 335-347.

[13] J. B. Julian, J. Ryan and R. A. Epstein, "Coding of Object Size and Object Category in Human Visual Cortex," *Cerebral Cortex,* vol. 27, pp. 3095-3109, 2017.

[14] P. K. Kaiser, The Joy of Visual Perception: A Web Book, York University, 1996.

[15] O. Braddick, "Neural Basis of Visual Perception," *International Encyclopedia of the Social & Behavioral Sciences,* pp. 16269-16274, 2001.

[16] T. J. Andrews, "Visual Cortex: How Are Faces and Objects Represented?," *Current Biology,* vol. 15, no. 12, pp. R451-R453, 2005.

[17] Y. Xu and M. M. Chun, "Visual grouping in human parietal cortex," *PNAS,* vol. 104, no. 47, pp. 18766-18771, 2007.

[18] B. Peters, J. Kaiser, B. Rahm and C. Bledowski, "Activity in Human Visual and Parietal Cortex Reveals Object-Based Attention in Working Memory," *J Neurosci,* vol. 35, no. 8, pp. 3360-3369, 2015.

[19] M. Vaziri-Pashkam and Y. Xu, "An Information-Driven 2-Pathway Characterization of Occipitotemporal and Posterior Parietal Visual Object Representations," *Cerebral Cortex,* pp. 1-17, 2018.

[20] K. Koenraadt, E. Roelofsen, J. Duysens and N. Keijsers, "Cortical control of normal gait and precision stepping: an fNIRS study," *Neuroimage,* vol. 85, no. 1, pp. 415-22, 2014.

[21] N. Naseer and K. Hong, "fNIRS-based brain-computer interfaces: A review," *Front. Hum. Neurosci,* vol. 9, no. 3, p. 10.3389/fnhum.2015.00003, 2015.

[22] P. Manoilov, "EEG eye-blinking artefacts power spectrum analysis," in *Proc. Int. Conf. Comput. Syst. Technol.*, 2006.

[23] A. Hyvarinen, J. Karhunen and E. Oja, Independent Component Analysis, New York / Chichester / Weinheim / Brisbane / Singapore / Toronto: JOHN WILEY & SONS, INC, 2001.

[24] A. De, T. Bhattacharjee, A. Konar, A. L. Ralescu and A. K. Nagar, "A type-2 fuzzy set induced classification of cognitive load in inter-individual working memory performance based on hemodynamic response," in *IEEE Symposium Series on Computational Intelligence (SSCI)*, Honolulu, HI, USA, 2017.

[25] A. De, A. Konar, A. Samanta, S. Biswas, A. L. Ralescu and A. K. Nagar, "Cognitive Load Classification in Learning Tasks from Hemodynamic Responses Using Type-2 Fuzzy Sets," in *IEEE International Conference on Fuzzy Systems (FUZZ-IEEE)*, Naples, Italy, 2017.

[26] A. D. Milner, "How do the two visual streams interact with each other?," *Exp Brain Res.,* vol. 235, no. 5, pp. 1297-1308, 2017.

[27] B. R. Sheth and R. Young, "Two Visual Pathways in Primates Based on Sampling of Space: Exploitation and Exploration of Visual Information," *Front. Integr. Neurosci,* p. 10.3389/fnint.2016.00037, 2016.

[28] M. N. Herbert and G. Hesselmann, "What Visual Information Is Processed in the Human Dorsal Stream?," *J Neurosci,* vol. 32, no. 24, pp. 8107-8109, 2012.

[29] S. Heim, K. Amunts, T. Hensel, M. Grande, W. Huber, F. Binkofski and S. B. Eickhoff, "The role of human parietal area 7A as a link between sequencing in hand actions and in overt speech production," *Front. Psychol.,* p. 10.3389/fpsyg.2012.00534, 2012.

[30] D. Milner and M. Goodale, The Visual Brain in Action, Oxford University Press, 2006.

[31] R. Thangavel, S. K. Sahu, G. W. Van Hoesen and A. Zaheer, "Modular and laminar pathology of Brodmann's area 37 in Alzheimer's disease," *Neuroscience,* vol. 152, no. 1, pp. 50-55, 2008.

[32] J. D. Sheskin, Handbook of Parametric and Nonparametric Statistical Procedures, Chapman & Hall/CRC, 2000.